Article

Retrieval of Sea Surface Temperature from MODIS Data in Coastal Waters

Rosa Maria Cavalli

National Research Council (CNR), Research Institute for Geo-Hydrological Protection (IRPI) via della Madonna Alta 126, 06128 Perugia, Italy; rosa.maria.cavalli@irpi.cnr.it; Tel.: +39-075-501-422

Abstract: Accurate measurements of sea surface temperature retrieved from remote images is a fundamental need for monitoring ocean and coastal waters. This study proposes a method for retrieving accurate measurements of SST in coastal waters. The method involves the estimation of effect of total suspended particulate matter (SPM) concentration on the value of sea surface emissivity (SSE) and the inclusion of this effect in SSE value that is put into SST calculation. Data collected in three Italian coastal waters were exploited to obtain SST_{skin} and SSE values and to analyze SPM effects on SSE value. The method was tested on MODIS images. Satellite measurements of SST obtained with current operational algorithm, which does not require SSE value as explicit input, were compared with in situ values of SST_{skin} and RMSD is equal to 1.13 K. Moreover, SST data were retrieved with an algorithm for retrieving SST measurements from MODIS data, which allows the inclusion of SSE value with SPM effect. These data were compared with in situ values of SST_{skin}, and RMSD is equal to 0.68 K.

1. Introduction

Coastal waters are very important for human populations because we derive a lot of benefits from these habitats: food (e.g., most caught fish come from the coastal waters and adjacent upwelling areas), renewable and nonrenewable resources (e.g., hydrocarbons and extracted sand and gravel), and services such as transportation, waste disposal, and recreation. In an assessment of world's ecosystems, the largest value in the whole ecosystem was assigned to the coastal waters [1]. On the other hand, these valuable areas have become very sensitive to impact from human activities. Human threats to the coastal areas fall into four categories: effects of contaminants, eutrophication, habitat loss, and overexploitation of fisheries resources [2]. Therefore, monitoring water quality, pollution assessment, and remediation are the most pressing requirements for ensuring sustainability of these valuable and vulnerable habitats [3–5].

Sea surface temperature (SST) measurements retrieved from remote images are used to analyze these valuable and vulnerable habitats, e.g., environmental conditions of benthic marine organisms [6,7], ground water discharges [8], interactions between residual circulation, tidal mixing and fresh influence [9], karstic springs [10], river plumes [11], thermal plume contamination [12–14], upwelling phenomena [15], and water quality [16]. Nevertheless, error, defined as the difference between some idealized "true value" and the measured value [17], in SST measurements is highlighted in different coastal regions by several studies, e.g., China [13], Western Australia [7], South Africa [18], and the US [7]. This error can be as large as 6 °C [18].

Another confirmation of the importance of accurate satellite measurements of SST is the series of infrared radiometers that were launched after the first Advanced Very High Resolution Radiometer (AVHRR) [19]. Among these, two Moderate Resolution Imaging Spectroradiometers (MODIS) of NASA's

Earth Observation System (EOS) constellation were designed for accurate measurements of SST: the first one on the Terra satellite was launched on 18 December 1999, and the second one on the Aqua satellite was launched on 4 May 2002 [20]. These instruments continue to produce an available "collection" of SST measurements. Collection specifically represents a revision of the instrument calibration model and the algorithm for SST retrieving [21]. Previous studies emphasize that the error in SST measurements can occur for many reasons and that each adjustment to reduce the error in SST measurements is important [22–27]. Each step of data acquisition and data processing is prone to additional error sources, such as atmospheric correction errors, e.g., [28,29], cloud contamination, e.g., [25,27], representativeness errors, e.g., [25,26], sampling errors, e.g., [22,23,26], and surface emissivity, e.g., [30,31]. The succession of the "collections" clearly demonstrates the importance of providing accurate measurements and of exploiting each adjustment that can reduce the error [19–27,32,33]. The operational algorithm for retrieving SST from MODIS images is a derivative of the split window technique, which corrects the atmospheric absorption of radiation between sea surface and satellite with brightness temperature differences at a few adjacent infrared bands [21,25,27,32,34]. Therefore, algorithm coefficients also include the impact of differences in column water vapor and SSE values. The split window algorithm for retrieving SST from MODIS images which was proposed by Niclos et al. [35] incorporates separate terms for column water vapor and SSE value. Sobrino et al. [28] already showed that including column water vapor in the split-window algorithm improves SST accuracy. Niclos et al. [35] considered that SST accuracy is improved by including column water vapor value and SSE value in the operational algorithm because the variation in SSE values is comparable to the variation in emissivity value of other land surfaces [35]. Some authors [30,36–40] proposed models for calculating SSE values. As shown by these models, SSE value is a function of sediment and salinity concentrations and zenith observation angles. Moreover, sea surface roughness, which is a function of sea surface wind speed, affects SSE value. Other authors [31,41–44] obtained SSE value from experimental data in order to improve the knowledge of SSE behavior and to develop and validate models. A reference work for all these studies is the paper written by Masuda et al. [30]. Based on Cox and Munch [45], the authors highlighted that the greatest effect of surface wind on emissivity is observed with surface wind speed greater than 15 m/s and zenith observation angle greater than 50° [30]. All these papers were mainly focused on open sea waters, whereas only a few studies [46–50] were concentrated on SSE behavior in coastal waters. The previous papers highlight that SSE value is affected by changes in refractive index, which can also be due to variation in concentration of total suspended particulate matter (SPM) [30,31,36–44,46,50]. Coastal waters are characterized by greater concentrations of SPM than open sea waters. This characteristic is due to human activities and the runoff of rivers, and it is so important that its contribution to the optical properties was defined as "dominant" [51]. Therefore, Wen-Yao et al. [46] and Wei et al. [49] specifically retrieved SSE behaviors with respect to SPM concentrations from measurements of thermal radiometers at 8–14 μm in laboratory. They agreed that SSE value decreases with increase in SPM concentrations that were included in the water samples [46,49]: the decrease is tiny for small concentrations and significant for large concentrations. However, the authors did not analyze SSE behaviors with respect to SPM concentration from 0 to 100 mg/L (i.e., the first addition of sediment is 100 mg/L). Yao et al. [46] highlighted that SSE value decreases with the first addition of sediment (i.e., 100 mg/L), remains at the same value up to 10,000 mg/L, and then falls again.

Besides great concentration of SPM, coastal waters are also characterized by greater variations in SPM composition, salinity, and sea surface wind speed than open sea waters [52]. The effects of SPM composition and salinity on SSE values was, respectively, analyzed in the laboratory by Salisbury [47] and Newman et al. [42]. SSE behaviors with respect to sea surface wind speed was calculated by Masuda et al. [30], Masuda [36], and Watts et al. [39]. SSE behaviors with respect to these variables were evaluated in stable environment where variation in each variable was under strict control [30,36,39,42,46,47,49]. Coastal waters cannot be defined as a stable environment [52].

This study develops and tests a method for retrieving accurate measurements of SST in the coastal waters. This method is based on the inclusion of column water vapor value and the effect

of SPM concentration on SSE value. This effect was estimated from data collected in coastal waters. SSE behavior with respect to SPM concentration confirms that SSE values decrease with increase in SPM concentration [46,49]. SST_{skin} measurements, which were obtained from in situ data, were compared with SST measurements retrieved from MODIS data with and without the inclusion of effect of SPM concentration. The comparison shows that the inclusion of these effects minimizes the error in SST measurements retrieved from remote images.

2. Materials

2.1. Study Area

A cruise was performed to characterize waters of the Manfredonia Gulf, the Taranto Gulf, and the area close to Lesina Lagoon during the summer of 2011 [53]. The Manfredonia Gulf is situated in the western part of the southern Adriatic Sea (Figure 1). Urban and agricultural activities in this area are considered potential threats to coastal marine ecosystem [54]. Fifteen measurement locations situated at distance of about 4 km from the coastline and between bathymetric lines of 10 m and 15 m were selected for describing these waters (Figure 1). Sampling of these locations were carried out during four days, and principal locations were monitored several times: in total, 39 water columns were analyzed. Each water column highlighted unique features, even though it was examined in the same position during different days. The waters of the Manfredonia Gulf were described with 39 different cruise locations.
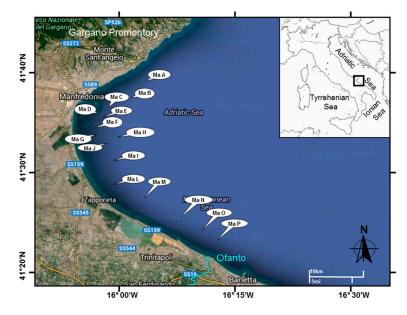

Figure 1. Measurement locations of the Manfredonia Gulf. Study area location (black box) in the top right.

The Taranto Gulf, which is located in the Ionian Sea (Figure 2), represents an example of coastal marine ecosystem where biological balances have been altered by industrial development, i.e., iron and steel factories, petroleum refineries, and shipyards [55]. Because their impact on environment is great, the Taranto province was officially classified as an "Area of High Environmental Risk" [56] and later was also included in the 14 "Sites of National Interest" that need to be remediated [57]. Seven measurement locations situated at different distance from the coastline (i.e., from 2 to 12 km) and at different depths (i.e., from 23 to 303 m) were chosen to analyze these waters (Figure 2). All these locations were monitored three times during four days for a total of 21 water columns. Each water column highlighted unique features, even though it was monitored in the same position during different days. The Taranto Gulf was described with 21 different locations.
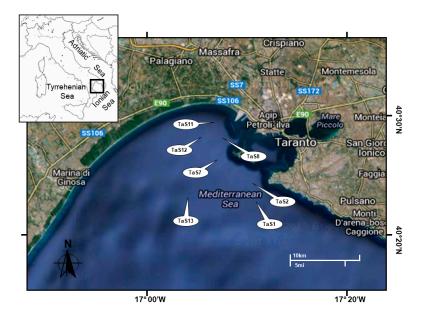
Figure 2. Measurement locations of the Taranto Gulf. Study area location (black box) in the top left.

Waters close to Lesina Lagoon are situated along the western part of the southern Adriatic Sea (Figure 3). The lagoon is characterized by shallow water, i.e., from 0.75 to 1.5 m, and a limited sea-lagoon exchange. Human intervention influences environment quality and determines the main factors of impact such as accumulation of nutrients, introduction of opportunistic species, protection of sea-lagoon exchange, and commercial activities of fishing and aquaculture [58]. Six measurement locations situated at a distance of about 10 km from the coastline and around a bathymetric line of 20 m were selected for describing the waters close to Lesina Lagoon (Figure 3). Survey of these waters was performed during one day.
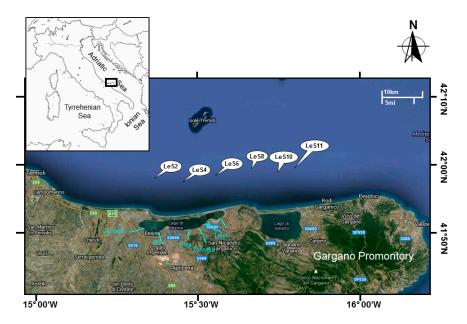

Figure 3. Measurement locations of coastal waters close to Lesina Lagoon. Study area location (black box) in the top left.

The position of all cruise observations was chosen in accordance with Mueller et al. [52] protocol and knowledge of these areas of study.

2.2. In Situ and Satellite Data

Waters of the Manfredonia Gulf, the Taranto Gulf, and the area close to Lesina Lagoon were analyzed during an oceanographic cruise [53] by means of collection and analysis of water samples, measurement of sea temperatures, calculation of salinity concentrations, and acquisition of thermal infrared radiances from the sea surface and sky. All in situ measurements were carried out from 5:40 to 17:30 UTC (Table 1).

Table 1. Date and time of the surveys and mean values of SST_{skin} and $SST_{subskin}$ estimated using Webster et al. [59] and Fairall et al. [60] models, respectively.

Coastal Waters of the Area Close to Lesina Lagoon					
Date	Start time (UTC)	End time (UTC)	Number of locations	Mean of SST_{Skin} by [59] (K)	Mean of $SST_{subskin}$ by [60] (K)
07 August 2011	7:30	16:00	6	300.12	300.14
Coastal Waters of the Manfredonia Gulf					
Date	Start time (UTC)	End time (UTC)	Number of Locations	Mean of SST_{Skin} by [59] (K)	Mean of $SST_{subskin}$ by [60] (K)
08 August 2011	7:01	15:20	6	301.25	301.27
09 August 2011	6:30	15:00	9	301.15	301.26
12 August 2011	7:50	16:10	10	299.79	299.99
24 August 2011	5:40	17:30	14	301.86	302.05
Coastal Waters of the Taranto Gulf					
Date	Start time (UTC)	End time (UTC)	Number of Locations	Mean of SST_{Skin} by [59] (K)	Mean of $SST_{subskin}$ by [60] (K)
13 August 2011	11:00	15:10	5	299.46	299.59
14 August 2011	7:05	14:30	7	300.25	300.34
15 August 2011	7:00	14:00	7	299.81	299.99
16 August 2011	10:00	14:00	2	299.95	300.02

In accordance with protocols laid down by Mueller et al. [61] and Pegau et al. [62], water samples were analyzed in the laboratory for calculating SPM concentrations. SPM concentrations were retrieved from superficial water samples. In accordance with Mueller et al. [52] protocol, each water column was classified as coastal water because SPM concentration of each one is more than 0.5 mg/L (Table 2).

Table 2. Values of mean and standard deviation (σ) of total suspended particulate matter (SPM) and salinity concentrations and sea surface emissivity (SSE) values with and without SPM effect, i.e., SSE (SPM ≠ 0) and SSE (SPM = 0) respectively.

Coastal Waters of	SPM (mg/L)		Salinity (g/L)		SSE (SPM ≠ 0)		SSE (SPM = 0)	
	Mean	σ	Mean	σ	Mean	σ	Mean	σ
the Manfredonia Gulf	5.07	2.36	38.30	0.11	0.975	0.003	0.981	0.003
the Taranto Gulf	2.15	0.60	38.30	0.04	0.975	0.001	0.978	0.001
area close to Lesina Lagoon	1.50	0.41	37.86	0.08	0.981	0.001	0.984	0.001

Sea temperature measurements of each location were acquired with three multi-parametric platforms: SeaBird Electronics SBE 911-plus Conductivity-Temperature-Depth (CTD), ELFO, which is equipped with Falmouth C-T sensor to measure sea temperature [63] and TFLAP, which acquires sea temperature with MicroTSG (MicroThermosalinograph) SBE 45 sensor [64]. Data were processed in accordance with UNESCO standards [65].

Thermal infrared radiances were obtained with an infrared camera: an FLIR Systems FLIR B series 360. FLIR records brightness temperature at wavelengths from 7.5 to 13 μm and has a sensitivity of 0.05 K at 30 °C and an accuracy of ±2%. The calibrations were carried out before and after the campaign to understand the stability of the instrumentation. In order to estimate SSE value, the previous studies [25–52] and the user's manual ThermalCAM Reseacher Professional [66] provide a useful procedure for detecting thermal infrared radiances. This procedure was thoroughly applied for each acquisition. (*i*) Radiance was measured, under specific conditions of weather (i.e.,

clear-sky and sea surface wind speed less than 5 m/s) from the deck of ship over sea portion where the multi-parametric platform was dived. (*ii*) The radiometer was alternately pointed downward to view the sea and upward to view the sky at required zenith angle θ equal to 45° and at required azimuth angle φ equal to 90° or 180°, where φ was calculated with respect to sun's azimuth and ship's heading should point the sun, i.e., azimuth angle equal to 0°. In order to verify the view angle, the radiometer equipped with a goniometer was mounted on a fixed position. (*iii*) Each pair of radiance measurements from sea and sky was simultaneously acquired with measurements of sea temperature; atmosphere temperature and relative humidity and sea surface wind speed were measured from each location.

The MODIS on board the Aqua satellite acquired nine images during the oceanographic cruise. The MODIS data were obtained from NASA's Distributed Active Archive Centers. In accordance with the previous papers [25–52,66], each location selected from MODIS images has a zenith observed angle smaller than 50°, and the greatest zenith observed angle is about 50° (i.e., the observations of the coastal water of the Manfredonia acquired on 14 August 2011).

3. Estimation of Sea Surface Skin Temperature Value from in Situ Data

Infrared radiometers (i.e., in situ and satellite) acquire the brightness temperature at surface skin layer of the water column (SST_{skin}), which is thin (about 500 μm), whereas sensors mounted on buoys, profiles, and ships measure sea temperature at any depth beneath the skin (SST_{dept}) [67]. The vertical temperature structure of the upper ocean such as coastal waters is variable; therefore, the quality of SST observations depends on the vertical position of the measurement within the water column and on the time of the day at which the measurements were obtained [68,69]. Consequently, some authors developed models for estimating diurnal and nocturnal warming at a specific depth [70].

Since three multi-parametric platforms measure SST_{depth}, their data were exploited to estimate SST_{skin} values using the empirical parametric model for retrieving diurnal SST_{skin} measurements proposed by Webster et al. [59]. This algorithm was selected because it was extensively compared with in situ measurements under light-to-moderate wind conditions [70–73]. It has the following form:

$$\Delta T = SST_{skin} - SST_{depth} = \text{f} + a(PS) + b(P) + c[\ln(u)] + d(PS)\ln u + e(u) \tag{1}$$

where *PS* is the daily peak surface solar radiation in Wm^{-2}; *P* is the daily mean precipitation rate in mmh^{-1}; *u* is sea surface wind speed in m/s; and *a*, *b*, *c*, *d*, *e*, and f are the coefficients provided by Webster et al. [59] that are a function of sea surface wind speed. The authors highlighted that ΔT value values cannot exceed 3 K [59].

ΔT values were estimated with SST_{depth} values and sea surface wind speeds monitored during the cruise and with the daily peak surface solar radiations, which were obtained from aerosol robotic network (AERONET) data. Therefore, 198 measurements of SST_{depth} were analyzed to retrieve SST_{skin} values of 66 observations, and mean values of these results are shown in Table 1.

In order to validate estimated values of SST_{skin}, simplified method proposed by Fairall et al. [60] was selected because it was also extensively tested [70,73]. This algorithm calculates a value of SST (i.e., $SST_{subskin}$) that is assumed to be independent of the depth. A previous study highlighted that this value can highlight a little difference with respect to SST_{skin} value [70] because "the model assumes linear profiles of temperature and surface-stress-induced current in this warm layer" [60]. $SST_{subskin}$ values were evaluated using the following equation [70,74]:

$$T(z) = SST_{subskin} - \left(\frac{z - \delta}{D_T - \delta} \right)^v [SST_{subskin} - T(D_T)] \tag{2}$$

where *T*(z) is temperature profile in the warm layer; z is the depth; δ is the depth the skin layer; D_T is the depth of the warm layer; v is an empirical parameter which is equal to 1 [70–74]. Therefore, 198 measurements of sea temperature were exploited to evaluate $SST_{subskin}$ values of 66 observations and mean values of these results are shown in Table 1.

The retrieved values of $SST_{subskin}$ are slightly greater than SST_{skin} values in accordance with Kawai and Wada [70]. Root mean square deviation (RMSD) between $SST_{subskin}$ and SST_{skin} values is equal to 0.12 K.

SST_{skin} values were exploited to retrieve SSE values from brightness temperature data which were acquired with in situ radiometer and to validate the results of the proposed method for retrieving SST from MODIS data (Figure 4).
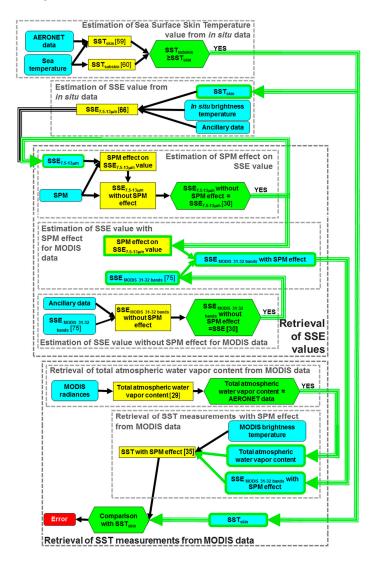

Figure 4. Flowchart of the applied method for retrieving SST measurements with SPM effect.

4. Estimation of SSE Value from in Situ Data

As above mentioned, SST_{skin} data allowed to retrieve SSE values from brightness temperature data that were acquired with in situ radiometer. Estimation of SSE values was performed by ThermalCAM QuikReport version 1.1., which employs the general formula used to all FLIR systems thermographic equipment [66]. This formula is based on the assumption that an instrument receives the radiation from the object itself and from the atmosphere surrounding the object. The received radiation is given by

$$W_{tot} = \varepsilon\tau W_{obj} + (1-\varepsilon)\tau W_{refl} + (1-\tau)W_{atm} \tag{3}$$

where $\varepsilon\tau W_{obj}$ is the emission from the object, which has a temperature equal to T_{obj}; ε is the emissivity of the object; τ is the transmittance of the atmosphere; $(1-\varepsilon)\tau W_{refl}$ is the reflected emission

from surrounding sources, which have the temperature equal to T_{refl}; $(1 - \tau)W_{atm}$ emission from atmosphere, which has the temperature equal to T_{atm}.

In accordance with the user's manual, each pair of radiance measurements acquired from sea surface and sky was processed together with the simultaneous SST_{skin} value, the relative humidity, and the atmosphere temperature. Each surface water was characterized by at least five sets of these variables. Each resultant value of SSE was compared with the others of the same station, and the values characterized by standard deviation smaller than 0.001 were taken into consideration. The mean of all these values was identified as the value of that station. The coastal waters of the Manfredonia Gulf, the Taranto Gulf, and the area close to Lesina Lagoon were described by 201 values of SSE for 39 observed locations, by 112 values of SSE for 21 observed locations, and by 28 values of SSE for six observed locations, respectively.

5. Retrieval of SSE Values

5.1. Estimation of SPM Effect on SSE Value

SSE behavior with respect to SPM concentration in the coastal waters of the Manfredonia Gulf, the Taranto Gulf, and the area close to Lesina Lagoon was derived from in situ data. The relationship between SSE and SPM in these coastal waters is well defined (Figure 5), and the following functions for adequately representing the data were found using optimal least squares fit (R^2 coefficients are equal to 0.865, 0.785, and 0.901, respectively) as follows:

$$SSE_{7.5-13\,\mu m}^{\text{Manfredonia Gulf}} = -0.0011\,\text{SPM} + 0.981 \tag{4}$$

$$SSE_{7.5-13\,\mu m}^{\text{Taranto Gulf}} = -0.0012\,\text{SPM} + 0.978 \tag{5}$$

$$SSE_{7.5-13\,\mu m}^{\text{area close to Lesina Lagoon}} = -0.0013\,\text{SPM} + 0.984 \tag{6}$$

where SPM is the concentration of total suspended particulate matter in mg/L.

The relationship between SSE values and salinity concentrations and the relationship between SSE values and sea surface wind speeds of these coastal waters cannot be adequately represented.

As above mentioned, the radiometer utilized consists of a single band in the range 7.5–13 μm, whereas MODIS bands 31 and 32 are extended from 10.78 to 11.28 μm and from 11.77 to 12.27 μm, respectively. Therefore, it is necessary to transform Equations (4)–(6) into algorithms for calculating SSE values with SPM effect in MODIS bands 31 and 32.

For this purpose, it is important to confirm that the Equations (4)–(6) evaluate SPM effect on SSE value. Since previous papers proposed models for estimating SSE values without SPM effect and with the effects of salinity concentration and surface wind speed zenith observation angle, e.g., [30,75], the decrease in SSE value associated with SPM concentration of each station was estimated with the Equations (4)–(6) and was added to SSE value derived from in situ radiance. All resultant values were compared with emissivity from 8 to 13 μm calculated with Masuda et al. [30] model (i.e., emissivity was evaluated with zenith observation angles equal to 40° and 50°, with wind speeds equal to 4 m/s and with salinity concentration from 37 to 39 g/L, Figure 4). SSE values tabulated by Masuda et al. [30] were selected because these values were only obtained with the inclusion of dissolved salt effect in the emissivity of the pure water and were confirmed by several authors [31,37–40,46,47]. The results of the comparison attest that SSE value of each station estimated without SPM effect is emissivity of sea water that is characterized by salinity of that station and by SPM concentration equal to 0 mg/L, $SSE_{7.5-13\ \mu m}$ (SPM = 0). Therefore, this comparison proves that SSE variation, which is evaluated with Equations (4)–(6), is mainly due to change of SPM. Thus, 0.981, 0.978 and 0.984 are the average values of $SSE_{7.5-13\ \mu m}$ (SPM = 0) of the coastal waters of the Manfredonia Gulf, the Taranto Gulf, and the area close to Lesina Lagoon, respectively (Figure 6, Table 2).
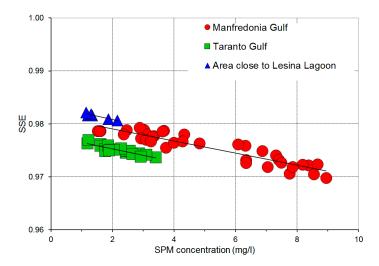
Figure 5. SSE behavior with respect to SPM concentration in these coastal waters.
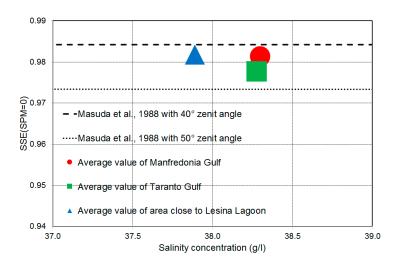

Figure 6. SSE values tabulated by Masuda et al. [30] and average values of the stations obtained without SPM effect versus salinity concentration.

In conclusion, the Equations (4)–(6) were rewritten into the following forms:

$$SSE_\lambda^{\text{Manfredonia Gulf}} = -0.0011 \, \text{SPM} \left(\frac{\text{SSE}_\lambda(SPM = 0)}{SSE_{7.5-13\,\mu\text{m}}(SPM = 0)} \right) + SSE_\lambda \, (SPM = 0) \qquad (7)$$

$$SSE_\lambda^{\text{Taranto Gulf}} = -0.0012 \text{SPM} \left(\frac{\text{SSE}_\lambda(SPM = 0)}{SSE_{7.5-13\,\mu\text{m}}(SPM = 0)} \right) + SSE_\lambda \, (SPM = 0) \qquad (8)$$

$$SSE_\lambda^{\text{area close to Lesina Lagoon}} = -0.0013 \, \text{SPM} \left(\frac{\text{SSE}_\lambda(SPM = 0)}{SSE_{7.5-13\,\mu\text{m}}(SPM = 0)} \right) + SSE_\lambda \, (SPM = 0) \qquad (9)$$

where λ is the spectral region.

5.2. Estimation of SSE Value without SPM Effect for MODIS Data

In order to obtain SSE in MODIS bands 31 and 32 with effect of SPM concentration ($SSE_{\text{MODIS\_band31}}$ ($SPM \neq 0$) and $SSE_{\text{MODIS\_band32}}$ ($SPM \neq 0$)), it is necessary to estimate *SSE* in these regions without this effect ($SSE_{\text{MODIS\_band31}}$ ($SPM = 0$) and $SSE_{\text{MODIS\_band32}}$ ($SPM = 0$)), since SPM concentrations are known (Equations (7)–(9)).

MODIS acquisitions over all stations on 14 August 2011 were performed with zenith observation angles larger than 50°, and SSE values tabulated with these angles by Masuda et al. [30] were not confirmed by some authors [31,37–39,43]. Therefore, SSE (SPM = 0) values in MODIS bands 31 and 32 were evaluated with the following equations proposed by Niclos and Caselles [75]:

$$SSE_{MODIS\_band\ 31}(\theta, U) = SSE_{MODIS\_band_{31}}(0°)\left[\cos\left(\theta^{cU+d}\right)\right]^{b_{31}} \tag{10}$$

$$SSE_{MODIS\_band_{32}}(\theta, U) = SSE_{MODIS\_band\ 32}(0°)\left[\cos\left(\theta^{cU+d}\right)\right]^{b_{32}} \tag{11}$$

where θ is zenith observation angle; U is sea surface wind speed in m/s; SSE_{MODIS_band31} $(0°)$ and SSE_{MODIS_band32} $(0°)$ are SSE values in MODIS bands 31 and 32, which were acquired with zenith observation angle equal to $0°$; c and d are constant coefficients (i.e., -0.037 ± 0.003 s/m and 2.36 ± 0.03); and $b31$ is equal to 0.0342; $b32$ is equal to 0.0508.

SSE_{MODIS_band31} $(0°)$ and SSE_{MODIS_band32} $(0°)$ values were obtained by Newman et al. [42] model. The authors investigated SSE behaviour with respect to the salinity concentration using in situ data and their results in MODIS bands 31 and 32 are confirmed by the SSE values of the most adopted models [30,76]. Therefore, SSE_{MODIS_band31} $(0°)$ and SSE_{MODIS_band32} $(0°)$ values are equal to 0.9922 and 0.9888, respectively.

SSE_{MODIS_band31} (SPM = 0) and SSE_{MODIS_band32} (SPM = 0) values of all stations were obtained with zenith observation angles retrieved from MODIS data and with sea surface wind speeds measured during the cruise. In order to confirm that these values are emissivity of each surface water characterized by its salinity and by SPM concentration equal to 0 mg/L, values estimated with Niclos and Caselles [75] equations were compared with SSE in 11 μm and 12 μm (i.e., MODIS bands 31 and 32) tabulated by Masuda et al. [30] (i.e., emissivity was obtained with zenith observation angle equal to the angle of each analyzed image, with wind speed equal to 4 m/s, and with salinity concentration equal to 38.26 g/L, i.e., average salinity, which was measured in situ, Figure 4). RMSD values between SSE_{MODIS_band31} (SPM = 0) and SSE_{MODIS_band32} (SPM = 0) values evaluated with Niclos and Caselles [75] equations and emissivity values calculated by Masuda et al. [30] are equal to 0.008 and 0.009, respectively. In accordance with the previous papers that did not confirm SSE values tabulated with angles larger than 50° by Masuda et al. [30,31,37–39,43], RMSD values of MODIS bands 31 and 32 acquired on 14 August 2011 are the largest, i.e., 0.020 and 0.017, respectively.

6. Retrieval of SST Measurements from MODIS Data

In order to test the method, locations monitored within ±2 h with respect to MODIS overpasses were selected, i.e., 56 locations (Table 3). The values of SST_{skin} that were obtained with the model proposed by Webster et al. [59] were compared with nearest pixels to ship locations obtained by MODIS Aqua Global Level 3 Mapped Thermal SST products at 4.63 km spatial resolution, which were provided by PO.DAAC FTP-site [77]. Values of RMSD, bias, and standard deviation (σ) are shown in Table 3.

Table 3. Comparisons (i.e., root mean square deviation (RMSD), bias and standard deviation, σ) between SST_{skin} data and SST measurements which were obtained by Moderate Resolution Imaging Spectroradiometers (MODIS) Aqua Global Level 3 Mapped Thermal SST products.

Coastal Waters of the Area Close to Lesina Lagoon					
Date Start Time	W (g/cm^2)	Number of Locations	Number of Locations Obtained from MODIS Level 3		SST (K) MODIS Level 3
07 August 2011 12:40 UTC	1.563	6	6	Bias	1.43
				σ	0.44
				RMSD	1.49

Table 3. *Cont.*

Coastal Waters of the Manfredonia Gulf					
Date Start Time	W (g/cm^2)	Number of locations	Number of Locations Obtained from MODIS Level 3		SST (K) MODIS Level 3
08 August 2011 11:45 UTC	5.246	5	2	Bias σ RMSD	1.12 0.64 1.21
09 August 2011 12:25 UTC	10.655	7	1	Bias σ RMSD	1.36 - -
12 August 2011 11:20 UTC	0.743	8	8	Bias σ RMSD	1.11 0.39 1.17
24 August 2011 11:40 UTC	2.103	11	7	Bias σ RMSD	0.20 0.11 1.26
Coastal Waters of Taranto Gulf					
Date Start Time	W (g/cm^2)	Number of Locations	Number of Locations Obtained from MODIS Level 3		SST (K) MODIS Level 3
13 August 2011 12:00 UTC	1.370	5	5	Bias σ RMSD	1.41 0.31 1.31
14 August 2011 12:45 UTC	1.517	6	1	Bias σ RMSD	1.33 - -
15 August 2011 11:50 UTC	0.743	6	7	Bias σ RMSD	0.98 0.43 1.06
16 August 2011 12:30 UTC	1.197	2	1	Bias σ RMSD	0.44 - -

The current operational procedure for deriving SST from MODIS data [21,24] is a regression to buoys data, which has not a value of SSE as an explicit term, whereas the split-window algorithm developed by Niclos et al. [35] includes SSE value. Therefore, this method was selected because it allows putting SSE value estimated with SPM effect into retrieval of SST measurements. MODIS images were exploit to retrieve SST measurements using the following equation [35]:

$$SST = T_{MODIS\_band_{31}} + [a_1(\sec\theta - 1) + a_2](T_{MODIS\_band31} - T_{MODIS\_band_{32}}) +$$
$$+ [b_1(\sec\theta - 1) + b_2](T_{MODIS\_band_{31}} - T_{MODIS\_band_{32}})^2 +$$
$$+ [c_1(\sec\theta - 1) + c_2] + (\alpha_0 + \alpha_1 w + \alpha_2 w^2)\left(1 - \frac{SSE_{MODIS\_band_{31}} + SSE_{MODIS\_band32}}{2}\right) +$$
$$- (\beta_0 + \beta_1 w + \beta_2 w^2)(SSE_{MODIS\_band31} - SSE_{MODIS\_band_{32}})$$

(12)

where T_{MODIS_bandi} is brightness temperature at satellite level in K; θ is zenith observation angle; w is total atmospheric water vapor content in g/cm^2; SSE_{MODIS_bandi} is sea surface emissivity in MODIS band; $a_1, a_2, b_1, b_2, c_1, c_2, \alpha_0, \alpha_1, \alpha_2, \beta_0, \beta_1, \beta_2$ are constant coefficients provided by Niclos et al. [35].

Brightness temperatures in MODIS bands 31 and 32 and zenith observation angle were derived from MODIS data; it was therefore necessary to calculate three input data: SSE_{MODIS_band31} (SPM $\neq$ 0), SSE_{MODIS_band32} (SPM $\neq$ 0) and total atmospheric water vapor content (Figure 4).

SSE_{MODIS_band31} (SPM $\neq$ 0) and SSE_{MODIS_band32} (SPM $\neq$ 0) values of each location were evaluated from in situ concentrations of SPM with the Equations (7)–(9) and with the method which was proposed by Wen-Yao et al. [46].

Total atmospheric water vapor content was retrieved from MODIS data using the following algorithm proposed by Sobrino et al. [29]:

$$w = 0.0192W_{MODIS\_band17} + 0.453W_{MODIS\_band18} + 0.355W_{MODIS\_band19}$$

(13)

with

$$W_{MODIS\_band17} = 26.314 - 54.434\frac{L_{MODIS\_band17}}{L_{MODIS\_band2}} + 28.449\left(\frac{L_{MODIS\_band17}}{L_{MODIS\_band2}}\right)^2 \quad (14)$$

$$W_{MODIS\_band18} = 5.012 - 23.017\frac{L_{MODIS\_band18}}{L_{MODIS\_band2}} + 27.884\left(\frac{L_{MODIS\_band18}}{L_{MODIS\_band2}}\right)^2 \quad (15)$$

$$W_{MODIS\_band19} = 9.446 - 26.887\frac{L_{MODIS\_band19}}{L_{MODIS\_band2}} + 19.914\left(\frac{L_{MODIS\_band19}}{L_{MODIS\_band2}}\right)^2 \quad (16)$$

and where w is total atmospheric water vapor content in g/cm^2 and L_{MODIS_bandi} is the radiance in $W\,m^{-2}\,sr^{-1}\,\mu m^{-1}$. Table 4 shows the results of each MODIS image. The results were compared with the values of precipitable water that were obtained from AERONET data (Figure 4). The best fit logarithmic curve between total atmospheric water vapor content and precipitable water values was identified in accordance with Mavromatakis et al. [78], and its R^2 is equal to 0.717.

Therefore, SST measurements at nearest pixels to ship locations were obtained with and without the inclusion of SPM effects in SSE values which were used as input into Niclos et al. [35] algorithm (Figures 4 and 7). In order to analyze the capability of SPM effect to minimize error in SST measurements, the included effects were obtained with Equations (7)–(9) and with the model proposed by Wen-Yao et al. [46]. The resultant data were compared with SST_{skin} values obtained with the model proposed by Webster et al. [59] (Table 4).
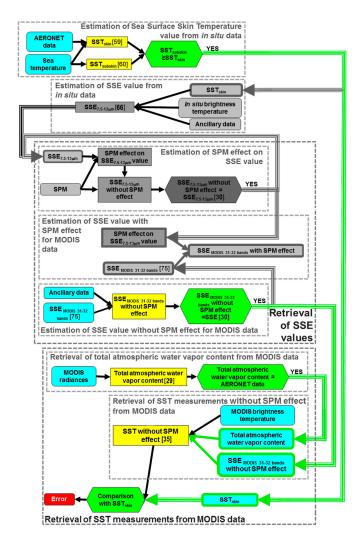

Figure 7. Flowchart of the applied method for retrieving SST measurements without SPM effect.

Table 4. Total atmospheric water vapor content values and comparisons (i.e., RMSD, bias and standard deviation, σ) between SST$_{skin}$ data and SST measurements at nearest pixels to ship locations which were retrieved from MODIS data using Niclos et al. [35] algorithm with and without the inclusion of SPM effects in SSE values. The included effects were evaluated with Equations (7)–(9) and with the method proposed by Wen-Yao et al. [46].

Coastal Waters of the Area Close to Lesina Lagoon						
				SST (K) Retrieved by [35]		
Date Start Time	W (g/cm²)	Number of Locations		with SSE (SPM = 0)	with SSE (SPM ≠ 0) Using Equations (7)–(9)	with SSE (SPM ≠ 0) Using Wen-Yao et al. [46]
07 August 2011 12:40 UTC	1.563	6	Bias	−0.49	−0.40	−0.49
			σ	0.48	0.50	0.48
			RMSD	0.66	0.60	0.66
Coastal Waters of the Manfredonia Gulf						
				SST (K) Retrieved by [35]		
Date Start Time	W (g/cm²)	Number of Locations		with SSE (SPM = 0)	with SSE (SPM ≠ 0) Using Equations (7)–(9)	with SSE (SPM ≠ 0) Using Wen-Yao et al. [46]
08 August 2011 11:45 UTC	5.246	5	Bias	−0.80	−0.65	−0.72
			σ	0.48	0.43	0.43
			RMSD	0.91	0.76	0.82
09 August 2011 12:25 UTC	10.655	7	Bias	−0.73	−0.67	−0.72
			σ	1.09	1.09	1.09
			RMSD	1.26	1.23	1.26
12 August 2011 11:20 UTC	0.743	8	Bias	−0.81	−0.50	−0.79
			σ	0.52	0.46	0.52
			RMSD	0.95	0.66	0.93
24 August 2011 11:40 UTC	2.103	11	Bias	−0.71	−0.29	−0.69
			σ	0.31	0.31	0.31
			RMSD	0.77	0.42	0.75
Coastal Waters of Taranto Gulf						
				SST (K) Retrieved by [35]		
Date Start Time	W (g/cm²)	Number of Locations		with SSE (SPM = 0)	with SSE (SPM ≠ 0) Using Equations (7)–(9)	with SSE (SPM ≠ 0) Using Wen-Yao et al. [46]
13 August 2011 12:00 UTC	1.370	5	Bias	−1.03	−0.89	−1.03
			σ	0.12	0.15	0.12
			RMSD	1.04	0.89	1.03
14 August 2011 12:45 UTC	1.517	6	Bias	−0.54	−0.42	−0.54
			σ	0.25	0.24	0.25
			RMSD	0.59	0.48	0.59
15 August 2011 11:50 UTC	0.743	6	Bias	−0.73	−0.59	−0.72
			σ	0.31	0.31	0.32
			RMSD	0.78	0.65	0.78
16 August 2011 12:30 UTC	1.197	2	Bias	−0.52	−0.41	−0.51
			σ	0.07	0.08	0.07
			RMSD	0.52	0.42	0.52

7. Sensitivity Analysis

Sensitivity analysis was aimed at assessing the error in SST measurements in coastal waters due to the omission of SPM effect from the estimation of SSE value. The error is the difference between SST obtained with and without the inclusion of SPM effect in SSE value. These two SSE values are specifically put into Niclos et al. [35] algorithm for retrieving SST from MODIS data using different total atmospheric water vapor content. The relative influence of SPM concentration and total atmospheric water vapor content on the error in SST measurements was calculated, and the zenith observation angle was set equal to 45° because its effect on SST measurements can be considered negligible.

SPM effect was derived from the increase in SPM concentration from 0 to 10 mg/L because this range was monitored in these coastal waters. SSE values were obtained from this range of concentrations with the Equations (7)–(9). Total atmospheric water vapor content was varied from 0.1 to 10 g/cm² because this range includes all values derived from MODIS images (Table 3).
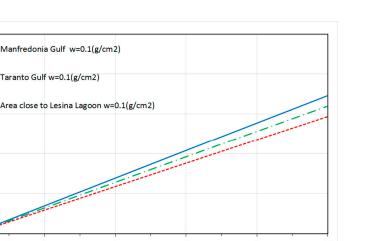
Figure 8 shows the behavior of the error in SST measurements with respect to the error due to the omission of SPM effect from the estimation of SSE value.
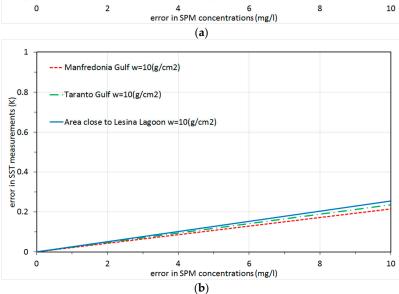
(**a**)

(**b**)

Figure 8. The error in SST measurements due to the omission of SPM effect from the estimation of SSE value: (**a**) the values obtained with total atmospheric water vapor contents (w) equal to 0.1 g/cm^2 is contained in the first panel; (**b**) the values obtained with w equal to 10 g/cm^2 is contained in the second panel.

8. Discussion and Conclusions

The paper aims to propose a method for retrieving accurate measurements of SST (Figure 4) and to demonstrate that the inclusion of the effect of SPM concentration in SSE value, which is put into the algorithms, minimizes the error in SST measurements, especially in coastal waters. For this purpose, an oceanographic cruise was performed to survey the coastal waters of the Manfredonia Gulf, the Taranto Gulf, and the area close to Lesina Lagoon, and 66 observations of water column were performed. Data collected in situ allowed for the estimation of SST$_{skin}$ and SSE values, the analysis of SSE behavior with respect to SPM concentration, and the validation of the results of the proposed method. Data acquired during the cruise by MODIS on board Aqua satellite was exploited to test the method.

SST$_{skin}$ values were estimated with the empirical parametric model for retrieving diurnal measurements of SST$_{skin}$ proposed by Webster et al. [59]. Moreover, SST$_{subskin}$ values were obtained with the simplified method for retrieving diurnal measurements of SST$_{subskin}$ proposed by Fairall et al. [60] in order to evaluate the SST$_{skin}$ values. These algorithms were chosen because they were extensively tested and were successfully applied [70,72,73]. Therefore, 198 measurements of sea temperature were exploited to retrieved 66 values of SST$_{skin}$ and SST$_{subskin}$. In order to validate the

results, $SST_{subskin}$ data were compared with SST_{skin} values. In accordance with [70], $SST_{subskin}$ values are slightly greater than SST_{skin} values (i.e., RMSD is equal to 0.12 K).

In accordance with the procedure for detecting thermal infrared radiances [25–52,66], SSE values from 7.5 to 13 µm were retrieved from at least five sets of variables: radiance measurements acquired from sea surface and sky (i.e., first and second variables), the relative humidity and atmosphere temperature data collected in situ (i.e., third and fourth variables), and validated values of SST_{skin} obtained by [59] (i.e., fifth variable). Therefore, 66 values of SSE were averaged out from 341 estimated values. The standard deviation values were smaller than 0.001. In order to analyze SSE behaviors, these values of SSE were compared with SPM and salinity concentrations and with sea surface wind speeds monitored in the same location. Only SSE behavior with respect to SPM concentration is well defined.

In summary, the effect of SPM concentration on SSE value from 7.5 to 13 µm can be evaluated from in situ concentrations with the developed algorithms (i.e., Equations (7)–(9)), which adequately represent SSE behaviors with respect to SPM concentrations of the Manfredonia Gulf, the Taranto Gulf, and the area close to Lesina Lagoon (R^2 coefficients are equal to 0.865, 0.785, and 0.901, respectively).

SSE behaviors with respect to SPM concentrations of these three coastal waters are slightly different (Figure 5) because SSE value is affected by feature variability of the adjacent river basins and Adriatic and Ionian seas, which modifies refractive index [54,55,58,79,80].

In order to validate 66 values of SSE from 7.5 to 13 µm, these values without SPM effect were compared with SSE values calculated by [30], and these values are comparable (Figure 6). SSE values for MODIS bands 31 and 32 were evaluated with Niclos and Caselles [75] equations. In order to validate these values, the data were compared with SSE values which were calculated by [30] (RMSD values are equal to 0.008 for SSE_{MODIS_band31} and 0.009 for SSE_{MODIS_band32}).

SST_{skin} measurements monitored within ±2 h with respect to MODIS overpasses were selected to test the method, i.e., 56 values. These values were compared with SST data provided by MODIS level 3 products. RMSD is equal to 1.13 K (Table 3). Moreover, SST values were retrieved from MODIS data using Niclos et al. [35] algorithm, which allows for including SSE values with SPM effect. Total atmospheric water vapor content values, which are required by [35], were retrieved from MODIS data using algorithm proposed by Sobrino et al. [29]. The results were validated with AERONET data (R^2 is equal to 0.717). In order to analyze the capability of SPM effect to minimize the error in SST retrieval, SSE values were evaluated with two models for retrieving SPM effect: developed algorithms (i.e., Equations (7)–(9)) and the model proposed by [46]. Therefore, 56 measurements of SST_{skin} were compared with SST values obtained with the inclusion of these two data set using Niclos et al. [35] algorithm. Total values of RMSD are equal to 0.62 K and 0.84 K, respectively (Table 4 and Figure 9).

Coastal waters of	MODIS Aqua Global Level 3 Mapped Thermal SST data (K)	SST data (K) retrieved by [35]		
		with SSE (SPM=0)	with SSE (SPM≠0) using Wen-Yao at al. [46]	with SSE (SPM≠0) using Equations (7)-(9)
the Manfredonia Gulf	1.22	0.95	0.92	0.72
the Taranto Gulf	1.12	0.76	0.76	0.64
area close to Lesina Lagoon	1.49	0.66	0.66	0.60

Figure 9. RMSD values of these coastal waters between SST_{skin} data and SST measurements which were obtained by MODIS Aqua Global Level 3 Mapped Thermal SST products. RMSD values of these coastal waters between SST_{skin} data and SST measurements retrieved from MODIS data using Niclos et al. [35] algorithm with and without the inclusion of SPM effects in SSE values.

In all stations monitored within ±2 h with respect to MODIS overpasses, SST retrieved from MODIS images with this inclusion using Niclos et al. [35] algorithm exhibits a reduction in error. The decrease with respect to MODIS level 3 products is up to 2.67 K. It should be noted that MODIS level 3 products are characterized by 4.63 km spatial resolution; only a partial number of stations,

i.e., 40 locations over 56, (Table 3) was derived from these products, and standard MODIS SST algorithms do not perform well in coastal situations because the atmospheric correction algorithms are optimized for oceanic conditions [21].

Sensitivity analysis was performed to analyze the behavior of the error in SST measurements in the coastal waters with respect to the error in SPM concentration (i.e., the error in SST measurements if the SPM concentration is assumed to be zero). SST measurements were derived from MODIS data using Niclos et al. [35] algorithm. The analysis took into consideration the increases in SPM concentration from 0 to 10 mg/L and total atmospheric water vapor content from 0.1 to 10 g/cm^2. Sensitivity analysis shows that error as large as 0.69 K in SST measurements is associated with an error in SPM concentration equal to 10 mg/L and with total atmospheric water vapor content equal to 0.1 g/cm^2 and error as large as 0.25 K in SST measurements is associated with an error in SPM concentration equal to 10 mg/L and with total atmospheric water vapor content equal to 10 g/cm^2. The analysis highlights that the increase in total atmospheric water vapor content decreases the error [28,29].

In summary, the analysis confirms that SSE values decrease with the increase of the SPM concentrations, and this decrease is tiny [46,49]. Moreover, the results of the developed method highlight that the error in SST measurements in these coastal waters decreases with the inclusion of SPM effect in the estimation of SSE value, which is used as input into the retrieval of SST from MODIS data. Certainly, an achieved map is never the territory [81,82], and therefore, a model cannot fully represent the variability and the complexity of the territory. However, the results attest to the accuracy of the procedure to acquire and analyze the in situ data and the accuracy of the developed algorithms for estimating the effect of SPM concentration on SSE values in MODIS bands 31 and 32.

In conclusion, this paper demonstrates that the inclusion of the effect of SPM concentration in SSE value, which is put into the algorithms for retrieving SST from remote data, minimizes the error in SST measurements in coastal waters. It is shown that an estimation of SPM effect on SSE value provides a useful adjustment for minimizing this error.

Future work should aim to improve spatial variability of SST measurements in coastal waters: SST measurements calculated with SPM effect will be estimated at monitored locations and in the whole remote image. For this purpose, the best method for retrieving SPM concentrations of these coastal waters from remote data will be developed, and the uncertainties will carefully be analyzed. Therefore, SPM concentration and total atmospheric water vapor content will be retrieved from MODIS data, and these products will be included in the algorithm for retrieving SST measurements of coastal waters from MODIS data.

Conflicts of Interest: The author declares no conflict of interest.

References

1. Costanza, R.; de Groot, R.; Sutton, P.; van der Ploeg, S.; Anderson, S.J.; Kubiszewski, I.; Farber, S.; Turner, R.K. Changes in the global value of ecosystem services. *Glob. Environ. Chang.* **2014**, *26*, 152–158. [CrossRef]
2. Crain, C.M.; Halpern, B.S.; Beck, M.W.; Kappel, C.V. Understanding and managing human threats to the coastal marine environment. *Ann. N. Y. Acad. Sci.* **2009**, *1162*, 39–62. [CrossRef] [PubMed]
3. Ahuja, S. *Monitoring Water Quality: Pollution Assessment, Analysis, and Remediation*; Elsevier: Waltham, MA, USA, 2013; 379p.
4. Sala, O.E.; Chapin, F.S.; Armesto, J.J.; Berlow, E.; Bloomfield, J.; Dirzo, R.; Leemans, R. Global biodiversity scenarios for the year 2100. *Science* **2000**, *287*, 1770–1774. [CrossRef]

5. USCOP (US Commission on Ocean Policy). *An Ocean Blueprint for the 21st Century: Final Report of the US Commission on Ocean Policy*; US Commission on Ocean Policy: Washington, DC, USA, 2004. Available online: https://oceanconservancy.org/wp-content/uploads/2015/11/000_ocean_full_report-1.pdf (accessed on 31 July 2017).

6. Blanchette, C.A.; Miner Melis, C.; Raimondi, P.T.; Lohse, D.; Heady, K.E.; Broitman, B.R. Biogeographical patterns of rocky intertidal communities along the Pacific coast of North America. *J. Biogeogr.* **2008**, *35*, 1593–1607. [CrossRef]

7. Smale, D.A.; Wernberg, T. Satellite-derived SST data as a proxy for water temperature in nearshore benthic ecology. *Mar. Ecol. Prog. Ser.* **2009**, *387*, 27–37. [CrossRef]

8. McCaul, M.; Barland, J.; Cleary, J.; Cahalane, C.; McCarthy, T.; Diamond, D. Combining Remote Temperature Sensing with in-Situ Sensing to Track Marine/Freshwater Mixing Dynamics. *Sensors* **2016**, *16*, 1402. [CrossRef] [PubMed]

9. Thomas, A.; Byrne, D.; Weatherbee, R. Coastal sea surface temperature variability from Landsat infrared data. *Remote Sens. Environ.* **2002**, *81*, 262–272. [CrossRef]

10. Fusilli, L.; Palombo, A.; Cavalli, R.M.; Pignatti, S. Airborne thermal data for detecting karst water resources in the Kotor Bay. In Proceedings of the 33rd International Symposium on Remote Sensing of Environment (ISRSE 2009), Stresa, Italy, 4–8 May 2009; pp. 356–359.

11. De Boer, G.J.; Pietrzak, J.D.; Winterwerp, J.C. SST observations of upwelling induced by tidal straining in the Rhine ROFI. *Cont. Shelf Res.* **2009**, *29*, 263–277. [CrossRef]

12. Ahn, Y.H.; Shanmugam, P.; Lee, J.H.; Kang, Y.Q. Application of satellite infrared data for mapping of thermal plume contamination in coastal ecosystem of Korea. *Mar. Environ. Res.* **2006**, *61*, 186–201. [CrossRef] [PubMed]

13. Tang, D.; Kester, D.R.; Wang, Z.; Lian, J.; Kawamura, H. AVHRR satellite remote sensing and shipboard measurements of the thermal plume from the Daya Bay. nuclear power station. China. *Remote Sen. Environ.* **2003**, *84*, 506–515. [CrossRef]

14. Xing, Q.; Chen, C.Q.; Shi, P. Method of integrating Landsat-5 and Landsat-7 data to retrieve sea surface temperature in coastal waters on the basis of local empirical algorithm. *Ocean Sci. J.* **2006**, *41*, 97–104. [CrossRef]

15. Azzaro, F.; Cavalli, R.M.; Decembrini, F.; Pignatti, S.; Santella, C. Biochemical and dynamical characteristics of the Messina Straits water by means of hyperspectral data. In Proceedings of the Second International Asia-Pacific Symposium on Remote Sensing of the Atmosphere, Environment, and Space, Sendai, Japan, 23 January 2001; pp. 240–249. [CrossRef]

16. Diofantos, G.H.; Marinos, G.H.; Kyriacos, T.; Agapiou, A. Integration of micro-sensor technology and remote sensing for monitoring coastal water quality in a municipal beach and other areas in Cyprus. In Proceedings of the SPIE Remote Sensing for Agriculture, Ecosystems, and Hydrology, Berlin, Germany, 18 September 2009.

17. BIPM; IEC; IFCC; ILAC; ISO; IUPAC; IUPAP; OIML. Evaluation of Measurement Data—Guide to the Expression of Uncertainty in Measurement. International Organization for Standardization (ISO), 2008. Available online: http://www.bipm.org/en/publications/guides/gum.html (accessed on 31 July 2017).

18. Smit, A.J.; Roberts, M.; Anderson, R.J.; Dufois, F.; Dudley, S.F.; Bornman, T.G.; Bolton, J.J. A Coastal Seawater Temperature Dataset for Biogeographical Studies: Large Biases between In Situ and Remotely-Sensed Data Sets around the Coast of South Africa. *PLoS ONE* **2013**, *8*, e81944. [CrossRef] [PubMed]

19. Harries, J.E.; Llewellyn-Jones, D.T.; Minnett, P.J.; Saunders, R.W.; Zavody, A.M.; Wadhams, P.; Taylor, P.K.; Houghton, J.T. Observations of sea-surface temperature for climate research. *Philos. Trans. R. Soc. Lond. A Math. Phys. Eng. Sci.* **1983**, *309*, 381–395. [CrossRef]

20. Esaias, W.E.; Abbott, M.R.; Barton, I.; Brown, O.B.; Campbell, J.W.; Carder, K.L.; Clark, D.K.; Evans, R.H.; Hoge, F.E.; Gordon, H.R.; et al. An overview of MODIS capabilities for ocean science observations. *IEEE Trans. Geosci. Remote Sens.* **1998**, *36*, 1250–1265. [CrossRef]

21. Kilpatrick, K.A.; Podestá, G.; Walsh, S.; Williams, E.; Halliwell, V.; Szczodrak, M.; Brown, O.B.; Minnett, P.J.; Evans, R. A decade of sea surface temperature from MODIS. *Remote Sens. Environ.* **2015**, *165*, 27–41. [CrossRef]

22. Liu, Y.; Minnett, P.J. Sampling errors in satellite-derived infrared sea-surface temperatures. Part I: Global and regional MODIS fields. *Remote Sens. Environ.* **2016**, *177*, 48–64. [CrossRef]

23. Liu, Y.; Chin, T.M.; Minnett, P.J. Sampling errors in satellite-derived infrared sea-surface temperatures. Part II: Sensitivity and parameterization. *Remote Sens. Environ.* **2017**, *198*, 297–309. [CrossRef]

24. Kilpatrick, K.A.; Podesta, G.P.; Evans, R. Overview of the NOAA/NASA advanced very high resolution radiometer Pathfinder algorithm for sea surface temperature and associated matchup database. *J. Geophys. Res. Oceans* **2001**, *106*, 9179–9197. [CrossRef]

25. Brown, O.B.; Minnett, P.J.; Evans, R.; Kearns, E.; Kilpatrick, K.; Kumar, A.; Sikorski, R.; Závody, A. *MODIS Infrared Sea Surface Temperature Algorithm Algorithm Theoretical Basis Document*; Version 2.0; University of Miami: Coral Gables, FL, USA, 1999; 91p.

26. Kennedy, J.J. A review of uncertainty in in situ measurements and data sets of sea surface temperature. *Rev. Geophys.* **2014**, *52*, 1–32. [CrossRef]

27. Minnett, P.J.; Brown, O.B.; Evans, R.H.; Key, E.L.; Kearns, E.J.; Kilpatrick, K.; Kumar, A.; Maillet, K.A.; Szczodrak, G. Sea-surface temperature measurements from the Moderate-Resolution Imaging Spectroradiometer (MODIS) on Aqua and Terra. In Proceedings of the 2004 IEEE International Geoscience and Remote Sensing Symposium (IGARSS '04), Anchorage, AK, USA, 20–24 September 2004; Volume 7, pp. 4576–4579. [CrossRef]

28. Sobrino, J.A.; Li, Z.L.; Stoll, M.P. Impact of the atmospheric transmittance and total water vapor content in the algorithms for estimating satellite sea surface temperature. *IEEE Trans. Geosci. Remote Sens.* **1993**, *31*, 946–952. [CrossRef]

29. Sobrino, J.A.; El Kharraz, J.; Li, Z.L. Surface temperature and water vapour retrieval from MODIS data. *Int. J. Remote Sens.* **2003**, *24*, 5161–5182. [CrossRef]

30. Masuda, K.; Takashima, T.; Takayama, Y. Emissivity of pure and sea waters for the model sea surface in the infrared window regions. *Remote Sens. Environ.* **1988**, *24*, 313–329. [CrossRef]

31. Konda, M.; Imasato, N.; Nishi, K.; Toda, T. Measurement of the sea surface emissivity. *J. Oceanogr.* **1994**, *50*, 17–30. [CrossRef]

32. Kilpatrick, K.A. Climate Algorithm Theoretical Basis Document (C-ATBD): Pathfinder SST. CDRP-ATBD-0099 v2; 2013. Available online: http://www1.ncdc.noaa.gov/pub/data/sds/cdr/CDRs/Sea_Surface_Temperature_Pathfinder/AlgorithmDescription.pdf (accessed on 25 August 2017).

33. Kilpatrick, K.; Podesta, G.; Walsh, S.; Evans, R.; Minnett, P. *Implementation of Version 6 AQUA and TERRA SST Processing*; White Paper; University of Miami: Coral Gables, FL, USA, 2014.

34. McMillin, L.M. Estimation of sea surface temperatures from two infrared window measurements with different absorption. *J. Geophys. Res.* **1975**, *80*, 5113–5117. [CrossRef]

35. Niclòs, R.; Caselles, V.; Coll, C.; Valor, E. Determination of sea surface temperature at large observation angles using an angular and emissivity-dependent split-window equation. *Remote Sens. Environ.* **2007**, *111*, 107–121. [CrossRef]

36. Masuda, K. Influence of wind direction on the infrared sea surface emissivity model including multiple reflection effect. *Meteorol. Geophys.* **2012**, *63*, 1–13. [CrossRef]

37. Niclòs, R.; Valor, E.; Caselles, V.; Coll, C.; Sánchez, J.M. In situ angular measurements of thermal infrared sea surface emissivity—Validation of models. *Remote Sens. Environ.* **2005**, *94*, 83–93. [CrossRef]

38. Niclòs, R.; Caselles, V.; Valor, E.; Coll, C.; Sánchez, J.M. A simple equation for determing seasurface emissivity in the 3–15 μm region. *Int. J. Remote Sens.* **2009**, *30*. [CrossRef]

39. Watts, P.D.; Allen, M.R.; Nightingale, T.J. Wind speed effects on sea surface emission and reflection for the along track scanning radiometer. *J. Atmos. Ocean. Technol.* **1996**, *13*, 126–141. [CrossRef]

40. Wu, X.; Smith, W.L. Emissivity of rough sea surface for 8–13 μm: Modeling and verification. *Appl. Opt.* **1997**, *36*, 2609–2619. [CrossRef] [PubMed]

41. Fiedler, L.; Bakan, S. Interferometric measurements of sea surface temperature and emissivity. *Dtsch. Hydrogr. Z.* **1997**, *49*, 357–365. [CrossRef]

42. Newman, S.M.; Smith, J.A.; Glew, M.D.; Rogers, S.M.; Taylor, J.P. Temperature and salinity dependence of sea surface emissivity in the thermal infrared. *Q. J. R. Meteorol. Soc.* **2005**, *131*, 2539–2557. [CrossRef]

43. Niclòs, R.; Caselles, V.; Coll, C.; Valor, E.; Rubto, E. Autonomous Measurements of Sea Surface Temperature Using In Situ Thermal Infrared Data. *J. Atmos. Ocean. Technol.* **2004**, *21*, 683–692. [CrossRef]

44. Smith, W.L.; Knuteson, R.O.; Revercomb, H.E.; Feltz, W.; Howell, H.B.; Menzel, W.P.; Nalli, N.R.; Brown, O.; Brown, J.; Minnett, P.; et al. Observations of the infrared radiative properties of the ocean-implications for the measurement of sea surface temperature via satellite remote sensing. *Bull. Am. Meteorol. Soc.* **1996**, *77*, 41–51. [CrossRef]

45. Cox, C.; Munk, W. Measurement of the roughness of the sea surface from photographs of the sun's glitter. *JOSA* **1954**, *44*, 838–850. [CrossRef]

46. Wen-Yao, L.; Field, R.T.; Gantt, R.G.; Klemas, V. Measurement of the surface emissivity of turbid waters. *Remote Sens. Environ.* **1987**, *21*, 97–109. [CrossRef]

47. Salisbury, J.W. Emissivity of terrestrial materials in the 8–14 μm atmospheric window. *Remote Sens. Environ.* **1992**, *42*, 83–106. [CrossRef]

48. Park, J.H.; Na, S.I. SST and SS changes during Saemangeum seawall construction using Landsat TM and ETM imagery. *Proc. SPIE* **2010**, *7831*. [CrossRef]

49. Wei, J.A.; Wang, D.; Gong, F.; He, X.; Bai, Y. The Influence of Increasing Water Turbidity on Sea Surface Emissivity. *IEEE Trans. Geosci. Remote Sens.* **2017**, *55*, 3501–3515. [CrossRef]

50. Zhao, Y.S. *Principles and Methods of Remote Sensing Application*; Science Press: Beijing, China, 2003.

51. Morel, A. Optical modelling of the upper ocean in relation to its biogenous matter content (case 1 waters). *J. Geophys. Res.* **1988**, *93*, 10749–10768. [CrossRef]

52. Mueller, J.L.; Austin, R.W.; Morel, A.; Fargion, G.S.; McClain, C.R. *Ocean Optics Protocols for Satellite Ocean Color Sensor Validation. Volume I: Introduction. Background and Conventions*; Revision 4, NASA Tech. Memo. 2003-21621; NASA Goddard Space Flight Center: Greenbelt, MD, USA, 2003; pp. 1–56.

53. Cavalli, R.M.; Betti, M.; Campanelli, A.; Di Cicco, A.; Guglietta, D.; Penna, P.; Piermattei, V. A methodology to assess the accuracy with which remote data characterize a specific surface, as a Function of Full Width at Half Maximum (FWHM): Application to three Italian coastal waters. *Sensors* **2014**, *14*, 1155–1183. [CrossRef] [PubMed]

54. Fiesoletti, F.; Specchiulli, A.; Spagnoli, F.; Zappalà, G. A new near time monitoring network in the Gulf of Manfredonia-Southern Adriatic Sea. In *European Operational Oceanography: Present and Future, Proceedings of the 4th International Conference on EuroGOOS, Brest, France, 6–9 June 2005*; European Commission Research Directorate-General: Brussels, Belgium, 2005; pp. 782–792.

55. Meftah, M.B.; De Serio, F.; Mossa, M.; Petrillo, A.F.; Pollio, A. Numerical results of the pollutant spreading offshore Taranto (Italy). In Proceedings of the 33rd IAHR Congress: Water Engineering for a Sustainable Environment, Vancouver, BC, Canada, 9–14 August 2009.

56. Law n. 349 (1986). Istituzione del Ministero Dell'ambiente e Norme in Materia di Danno Ambientale. Gazzetta Ufficiale della Repubblica Italiana del 15 luglio 1986, n. 162, Supplemento Ordinario n. 59. Available online: http://www.minambiente.it/sites/default/files/legge_08_07_1986_349.pdf (accessed on 6 November 2017).

57. Law n. 426 (1998). Nuovi interventi in campo ambientale. Gazzetta Ufficiale della Repubblica Italiana del 14 Dicembre 1998, n. 291, Serie Generale. Available online: http://www.agentifisici.isprambiente.it/ (accessed on 6 November 2017).

58. Roselli, L.; Fabbrocini, A.; Manzo, C.; D'Adamo, R. Hydrological heterogeneity. nutrient dynamics and water quality of a non-tidal lentic eco system (Lesina Lagoon. Italy). *Estuar. Coast. Shelf Sci.* **2009**, *84*, 539–552. [CrossRef]

59. Webster, P.J.; Clayson, C.A.; Curry, J.A. Clouds, radiation, and the diurnal cycle of sea surface temperature in the tropical western Pacific. *J. Clim.* **1996**, *9*, 1712–1730. [CrossRef]

60. Fairall, C.W.; Bradley, E.F.; Hare, J.E.; Grachev, A.A.; Edson, J.B. Bulk parameterization of air–sea fluxes: Updates and verification for the COARE algorithm. *J. Clim.* **2003**, *16*, 571–591. [CrossRef]

61. Mueller, J.L.; McClain, G.; Bidigare, R.; Trees, C.; Balch, W.; Dore, J.; Drapeau, D.; Karl, D.; Van, L. *Ocean Optics Protocols for Satellite Ocean Color Sensor Validation. Revision 5. Volume V: Biogeochemical and Bio-Optical Measurements and Data Analysis Protocols*; NASA Tech. Memo. 2003-21621; NASA Goddard Space Flight Center: Greenbelt, MD, USA, 2003; pp. 1–36.

62. Pegau, S.; Zaneveld, J.R.V.; Mitchell, B.G.; Mueller, J.L.; Kahru, M.; Wieland, J.; Stramska, M. *Ocean Optics Protocols For Satellite Ocean Color Sensor Validation. Revision 4. Volume IV: Inherent Optical Properties: Instruments. Characterizations. Field Measurements and Data Analysis Protocols*; NASA Tech. Memo. 2003-211621; NASA Goddard Space Flight Center: Greenbelt, MD, USA, 2003; pp. 1–76.

63. Bonamano, S.; Piermattei, V.; Marcelli, M.; Peviani, M. Comparison Between Physical Variables Acquired by a New Multiparametric Platform, ELFO, and Data Calculated by a Three-Dimensional Hydrodynamic Model in Different Weather Conditions at Tiber River mouth (Latium coast, Italy). EGU General Assembly

Conference Abstracts, May 2010; Volume 12, p. 5226. Available online: http://meetingorganizer.copernicus.org/EGU2010/EGU2010-5226.pdf (accessed on 31 July 2017).

64. Marcelli, M.; Piermattei, V.; Madonia, A.; Lacava, T.; Mainardi, U. T-FLaP advances: Instrumental and operative implementation. *J. Oper. Oceanogr.* **2016**, *9*, s185–s192. [CrossRef]

65. Crease, J.; Dauphinee, T.; Grose, P.L.; Lewis, E.L.; Fofonoff, N.P.; Plakhin, E.A.; Striggow, K.; Zenk, W. *The Acquisition. Calibration and Analysis of CTD Data*; UNESCO Technical Papers in Marine Sciences, 54; UNESCO: Paris, France, 1988; pp. 1–105.

66. *User's Manual Thermal CAM Reseacher Professional—Professional Edition*; Version 2.9; FLIR Systems: Limbiate (MI), Italy, 2009.

67. Mueller, J.L.; Morel, A.; Frouin, R.; Davis, C.; Arnone, R.; Carder, K.; Lee, Z.P.; Steward, R.G.; Hooker, S.; Holben, B.; et al. *Ocean Optics Protocols For Satellite Ocean Color Sensor Validation. Revision 4. Volume III: Radiometric Measurements and Data Analysis Protocols*; NASA Tech. Memo. 2003-21621; NASA Goddard Space Flight Center: Greenbelt, MD, USA, 2003; pp. 1–84.

68. Donlon, C.; Rayner, N.; Robinson, I.; Poulter, D.J.S.; Casey, K.S.; Vazquez-Cuervo, J.; May, D. The global ocean data assimilation experiment high-resolution sea surface temperature pilot project. *Bull. Am. Meteorol. Soc.* **2007**, *88*, 1197–1213. [CrossRef]

69. Donlon, C.J.; Minnett, P.J.; Gentemann, C.; Nightingale, T.J.; Barton, I.J.; Ward, B.; Murray, M.J. Toward improved validation of satellite sea surface skin temperature measurements for climate research. *J. Clim.* **2002**, *15*, 353–369. [CrossRef]

70. Donlon, C.J.; Keogh, S.J.; Baldwin, D.J.; Robinson, I.S.; Ridley, I.; Sheasby, T.; Barton, I.J.; Bradley, E.F.; Nightingale, T.J.; Emery, W. Solid-State Radiometer Measurements of Sea Surface Skin Temperature. *J. Atmos. Ocean. Technol.* **1998**, *15*, 775–787. [CrossRef]

71. Kawai, Y.; Wada, A. Diurnal sea surface temperature variation and its impact on the atmosphere and ocean: A review. *J. Oceanogr.* **2007**, *63*, 721–744. [CrossRef]

72. Fairall, C.W.; Bradley, E.F.; Godfrey, J.S.; Wick, G.A.; Edson, J.B.; Young, G.S. Cool-skin and warm-layer effects on sea surface temperature. *J. Geophys. Res. Oceans* **1996**, *101*, 1295–1308. [CrossRef]

73. Gentemann, C.L.; Minnett, P.J.; Ward, B. Profiles of ocean surface heating (POSH): A new model of upper ocean diurnal warming. *J. Geophys. Res. Oceans* **2009**, *114*, C07017. [CrossRef]

74. Zeng, X.; Beljaars, A. A prognostic scheme of sea surface skin temperature for modeling and data assimilation. *Geophys. Res. Lett.* **2005**, *32*, L14605. [CrossRef]

75. Niclòs, R.; Caselles, V. Angular variation of the sea surface emissivity. In *Recent Research Development in Thermal Remote Sensing*; Research Signpost: Kerela, Indian, 2005; pp. 37–65.

76. Friedman, D. Infrared characteristics of ocean water (1.5–15 μ). *Appl. Opt.* **1969**, *8*, 2073–2078. [CrossRef] [PubMed]

77. PO.DAAC MODIS Level 3 Data User Guide, MODIS Dataset, Version 2014.0. Available online: ftp://podaac-ftp.jpl.nasa.gov/allData/modis/L3/docs/UserGuide_MODIS_L3_v2014.0.pdf (accessed on 1 February 2017).

78. Mavromatakis, F.; Gueymard, C.A.; Franghiadakis, Y. Improved total atmospheric water vapour amount determination from near-infrared filter measurements with sun photometers. *Atmos. Chem. Phys.* **2007**, *7*, 4613–4623. [CrossRef]

79. Polemio, M.; Dragone, V.; Limoni, P.P. Monitoring and methods to analyse the groundwater quality degradation risk in coastal karstic aquifers (Apulia, Southern Italy). *Environ. Geol.* **2009**, *58*, 299–312. [CrossRef]

80. Simeoni, U. I litorali tra Manfredonia e Barletta (Basso Adriatico): Dissesti, sedimenti, problematiche ambientali. *Boll. Soc. Geol. Ital.* **1992**, *111*, 367–398.

81. Korzybski, A. *Science and Sanity*; Science Press Printing: Lancaster, PA, USA, 1958.

82. Milella, M. *Esplorare le Frontiere verso una Interculturalitá Formativa*; Edizione Ateneo: Perugia, Italy, 2007.